RSC Applied Polymers

ROYAL SOCIETY OF CHEMISTRY

PAPER

View Article Online
View Journal | View Issue

Cite this: *RSC Appl. Polym.*, 2024, **2**, 434

3D printed modular piezoionic sensors using dynamic covalent bonds†

Julian Smith-Jones,[a] Nathan Ballinger,[a] Naroa Sadaba,[a] Xabier Lopez de Pariza,[b] Yunxin Yao,[c] Stephen L. Craig,[c] Haritz Sardon[b] and Alshakim Nelson *[a]

Received 22nd December 2023,
Accepted 9th February 2024

DOI: 10.1039/d3lp00289f

rsc.li/rscapplpolym

Flexible and lightweight sensors can assess their environment for a broad range of applications that include wearables for health monitoring and soft robotics. While 2D and 3D printing enables control over sensor design in multiple dimensions, customizability of a sensor toward different individual use cases is still limited because each sensor requires a new design and manufacturing process. Thus, there is a need for methodologies that produce modular sensor components that can be assembled and customized by an individual user. Herein, we demonstrate 3D printed, elastomeric ionogels comprising covalent adaptable networks (CANs) for modular sensor assemblies. Reversible Diels–Alder connections incorporated into the network can occur at the interface between two 3D printed objects in physical contact with each other. As a result, modular components can be combined and assembled on-demand into customized piezoionic sensors. Thermal curing of these modular blocks triggered the dynamic remodeling of the polymer networks that caused them to become fused together. Three different configurations (linear, cyclic, and box assemblies) were demonstrated to afford piezoionic sensors from the same set of 3D printed building blocks. This study highlights the benefits of dynamic covalent networks toward decentralized manufacturing, wherein a modular approach enables customization of 3D printed parts without the need for modifying the original design.

Introduction

Flexible electronic devices have gained significant interest as sensors for soft robotics,[1–6] artificial skins,[7–12] and biomedical monitors.[13–16] At a minimum, the operational device must be conductive, elastomeric, and maintain functionality after storage under ambient conditions. Traditional sensor materials such as carbon nanotubes,[17–19] liquid metals,[8,20,21] or organic field effect transistors (OFET)[22–25] show great promise, however, when placed inside a soft matrix such as silicone, these conductive elements often limit the amount of deformation the material can withstand. The trade-offs between electronic performance, device shape, and mechanical flexibility also place limitations on the implementation and versatility of these sensors. Furthermore, the form factor required by the end-user can be specific to a particular scenario (or use case), but each one may require a new manufacturing process. The ability for an end-user to build a sensor from a set of simple building blocks presents an opportunity for greater versatility, design flexibility, and rapid implementation of these sensors.

Ionic liquids (ILs) are organic salts that are liquid at ambient temperatures, and these functional solvents are attractive as components of flexible strain sensors.[1–3,5–7,9–15,26–29] ILs can swell polymer networks to form ionic liquid gels (ionogels),[11,30,31] which can have many similarities to water-swollen hydrogels.[7,8,10,16] The advantages of IL gels include their intrinsic ionic conductivity and their negligible vapor pressure that limits solvent evaporation. The chemical structures of ILs are highly tunable, and they can be made to be stable at elevated temperatures, which affords ionic sensors with a wide operational temperature range.[32,33] While the composition of the ionic liquid can have a significant effect upon the conductive performance of the material,[11] the polymer network can be optimized to enhance the mechanical properties. For example, Wang *et al.*[33] demonstrated that ionogels comprised of acrylamide and acrylic acid in 1-ethyl-3-methylimidazolium ethyl sulfate afforded tough ionogels (Young's modulus of 46.5 MPa). Zhao *et al.*[34] demonstrated a fluorescent double network ionogel strain sensor

[a]*The Department of Chemistry, University of Washington, Seattle, WA 98195, USA. E-mail: alshakim@uw.edu*
[b]*POLYMAT and Department of Polymers and Advanced Materials: Physics, Chemistry and Technology, Faculty of Chemistry, University of the Basque Country UPV/EHU, Paseo Manuel de Lardizabal 3, 20018 Donostia-San Sebastián, Spain. E-mail: haritz.sardon@ehu.es*
[c]*Department of Chemistry, Duke University, Durham, NC, 27708, USA. E-mail: stephen.craig@duke.edu*
† Electronic supplementary information (ESI) available. See DOI: https://doi.org/10.1039/d3lp00289f

which possessed self-healing properties due to dynamic imine bonds and hydrogen bonds. More recently, Chen *et al.*[35] demonstrated an ultra-tough ionic liquid gel with a Young's modulus of 325 MPa and strain at break of 1120%, in addition to modest self-healing due to dynamic transition metal cross-links. In all the examples discussed, the sensors were generated through traditional casting methods, which limits the range of potential form factors that can be easily fabricated.

3D printing has been gaining significant interest due to the ability to produce a complex part or product on demand.[36–44] In particular, vat photopolymerization 3D printing allows for facile fabrication of devices with complex geometries which would otherwise be inaccessible. Wang *et al.*[45] demonstrated an ionogel comprised of 1-vinyl-3-butylimidazolium tetrafluoroborate and acrylate-terminated hyperbranched polymer swelled with 1-butyl-3-methylimidazolium tetrafluoroborate. The resin produced strain sensors with high stretchability, sensitivity, and a wide operating temperature range. Hao *et al.*[9] developed an ultra-stretchable ionic skin (strain at break >10 000%) capable of sensing over a temperature range of −40 to 150 °C. The material comprised of poly (zwitterionic ionic liquid)-*co*-poly (acrylic acid) in 1-ethyl-3-methyl-imidazolium ethyl sulfate could be SLA 3D printed into sensors used for monitoring human hand motion. Jurinovs *et al.*[17] formulated an SLA 3D printable biobased IL gel by mixing 1-ethyl-3-methylimidazolium acetate with single walled carbon nanotubes (SWCNTs) in acrylated rapeseed oil. The combination of IL and SWCNT provided excellent conductivity and allowed the material to function as electrodes in soft robotics and flexible sensors. Recently, Narupai *et al.*[36] demonstrated an elastomeric, SLA printable ionogel containing 1-butyl-3-vinylimidazolium bis(trifluoromethanesulfonyl)imide and polyethylene glycol (PEG). The gels displayed good conductivity, high elastic recovery, and strong adhesive properties. While 3D printing is advantageous because new design iterations can be made easily using computer-aided design (CAD) software, a modular system based on building blocks that can be arbitrarily assembled post-3D printing would allow for the facile combination of individual components without the need to alter the original design.[46,47] Morin *et al.*[48] demonstrated the concept using "Click-e-bricks", which are elastomeric bricks fabricated through molding that can be connected by peg/recess click connections. The modular structures were pneumatically actuated, and by varying the shape of the bricks they were able to achieve different geometries and shape transformations. The designs are applicable to a range of materials (*e.g.*, PDMS, Ecoflex) and provide access to structures which would be difficult to create in one molding step. Gomez *et al.*[49] developed a thiol–acrylate resin which could be photopolymerized into self-healing elastomeric gels. SLA printing allowed the researchers to produce individual parts which could be combined using heat to produce modular elastomeric actuators. Extending this modular approach to sensors would not only enable personalized devices to be fabricated, but also would be advantageous under conditions where it may not be possible to know what form factor is required for the sensor.

Herein, we demonstrate 3D printed, elastomeric ionogels comprising covalent adaptable networks (CANs) for modular piezoionic sensor assemblies. CANs are covalently crosslinked polymer networks (*i.e.*, thermosets) which contain reversible covalent bonds that enable the network to rearrange in response to an external stimulus such as mechanical force, light, or heat.[50–55] We developed a resin for vat photopolymerization which afforded polymer networks comprising reversible Diels–Alder connections. The resins were formulated in ionic liquid solvents, and thus, the resulting networks were ionogels. The 3D printed components were elastomeric with failure strains ranging from 600% to 1200%, low hysteresis over multiple deformation cycles, and high sensitivity (gauge factor = 3.59). The thermal reversibility of the dynamic bonds enabled 3D printed components in physical contact to fuse together *via* remodeling of the polymer networks. Thus, the 3D printed parts could be assembled into any arbitrary design and perform as piezoionic sensors.

Results and discussion

Butyl–vinyl imidazolium bis(trifluoromethanesulfonyl)imide ([BVIM][TFSI]) is an ionic liquid that can be co-polymerized with dimethacrylate cross-linkers to form polymer networks (Fig. 1).[12,27,36] The vinyl substituent on the imidazolium is reactive to photo-initiated free radical polymerization, while the length of the alkyl substituent influences the resin viscosity of the uncured resin and the mechanical properties of the resulting network. We chose butyl as the alkyl chain based on the viscosity of the resin, as well as the viscoelasticity of the resulting polymer network (in general, as the length of the alkyl chain increases, Young's modulus decreases and the elongation at break increases).[27] Networks solely comprising of the polymerizable ILs are brittle,[27,36] but the presence of oligo- and poly-ethylene glycol (PEG) is known to reduce brittleness.[18,36] To introduce reversible Diels–Alder linkages into the polymer network, PEG cross-linker **DA-PEG 1** was synthesized (Scheme S1†). The telechelic polymer has reversible Diels–Alder adducts at each end, and the polymer is terminated by methacrylate functionalities to facilitate its incorporation into the polymer network. **DA-PEG-1** was synthesized from PEG (M_n = 8000 g mol^{-1}), which was transformed into a bis-maleimide terminated polymer. Separately, furfuryl methacrylate was synthesized by reacting furfuryl alcohol with methacrylic anhydride. The Diels–Alder reaction between furfuryl methacrylate and bis-maleimide terminated polymer was performed neat at 70 °C overnight to yield **DA-PEG-1**.

Resins for vat photopolymerization were formulated comprising cross-linker **DA-PEG-1**, [BVIM][TFSI], photoinitiator, and photoabsorber. The amount of **DA-PEG-1** included in the resins varied from 10, 15, to 20 w/w% to modulate the viscoelastic properties of the polymer network. The resin formulations were labelled according to the w/w% of polymer present (10-BVIM, 15-BVIM, and 20-BVIM). For example, a resin containing 10 w/w% **DA-PEG-1** dissolved in [BVIM][TFSI]

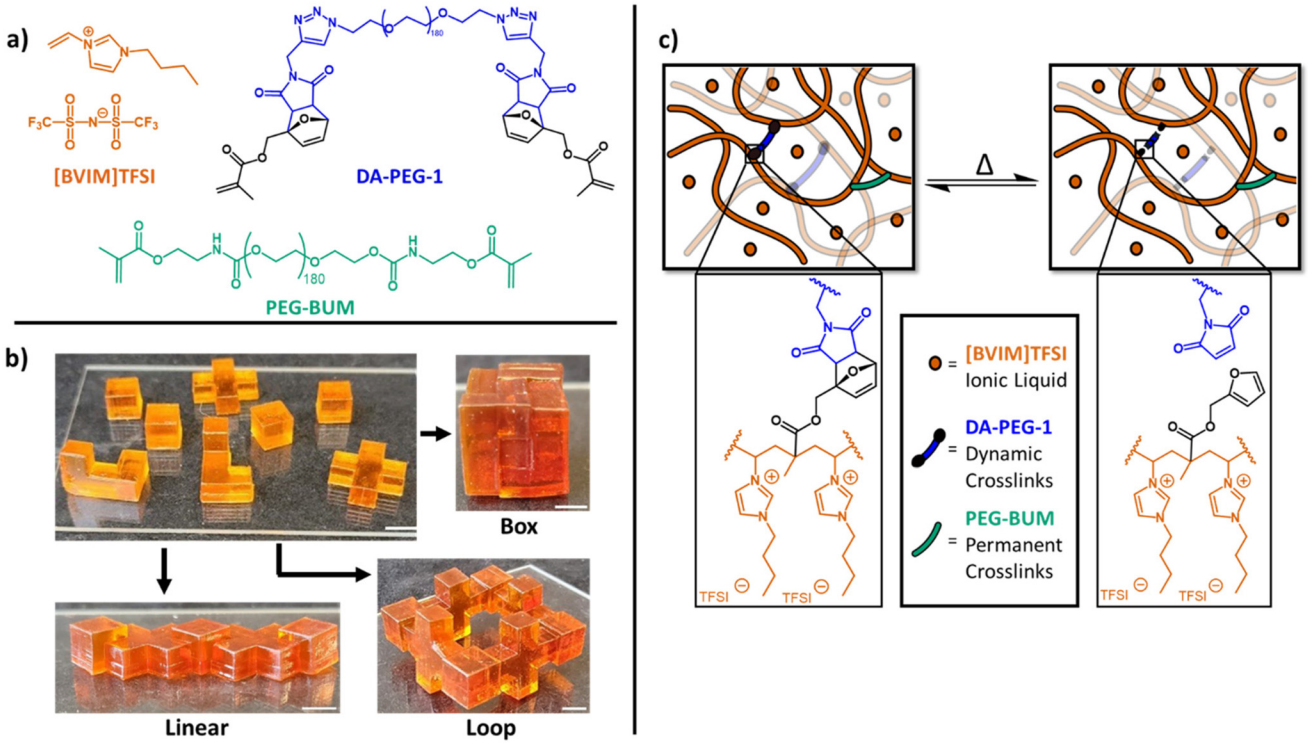

Fig. 1 Overview of resin components and representation of dynamic polymer network. (a) The network-forming components in the ionic liquid resin. The resin also includes BAPO (photoinitiator) and Sudan 1 (photoabsorber), which are not shown. (b) A vat photopolymerization process was used to fabricate modular building blocks (cube, cross, and bent arm) that were then assembled into a box, loop, or linear form. The building blocks are fused together using (c) the reversible Diels–Alder interactions that can occur at their interfaces. The mixture of dynamic and permanent crosslinks improved shape retention after heating.

was labeled 10-BVIM, while 20-BVIM corresponds to 20 w/w% **DA-PEG-1** in [BVIM][TFSI]. To further improve the structural integrity of the gels at elevated temperatures, we formulated a resin with a 1 : 1 ratio of the non-dynamic crosslinker PEG bis (urethane) methacrylate (PEG-BUM)[36,56] in addition to the dynamic crosslinker **DA-PEG-1** in [BVIM][TFSI] (we refer to this resin as 7.5–7.5-BVIM). Phenyl bis(2,4,6-trimethylbenzoyl) phosphine oxide (BAPO) was included (0.75 w/w%) as a photoinitiator in all of the formulations. Sudan I was included (0.025 w/w%) as a photoabsorber to improve the resolution during the printing process. Two important parameters to consider for SLA printing are the resin viscosity and rate of photocuring. It is important that the viscosity of the resin remains below 10 Pa s to allow the resin to flow properly during printing. The resin must also cure rapidly during printing to adhere to the build plate, while at the same time not polymerizing too quickly which may result in poorly resolved features. This can be controlled with the quantity of photoabsorber used in formulating the resin. The viscosity of the ionic liquid resins presented here were approximately 1 Pa s, well within the range required for printing.[36] The rheological properties of the resins are provided in the ESI (Fig. S12†).

Ionogels were 3D printed on a Formlabs Form 2 printer. Stereolithographic apparatus (SLA) 3D printing is a form of vat photopolymerization wherein a tray with a transparent base is filled with a photo-curable resin, and a 405 nm laser photopatterns cross-sectional areas of a 3D structure in a layer-wise fashion. Tensile specimens were printed to characterize mechanical properties, and modular building blocks were also printed to demonstrate the modularity of the system. All of the samples were subjected to a 1 h post cure in which both sides of the structure were irradiated with 405 nm light for 30 min each. Gel fraction experiments revealed that printed and cured specimens have a gel content of approximately 64.8% (Tables S2–S5†). The unpolymerized ionic liquid remaining in the networks is important because it contributes to the ionic conductivity and viscoelasticity of the materials, which enables the printed objects to function as strain sensors.

Fig. 2 shows the mechanical characterization data for the printed ionogels. Uniaxial tensile experiments were performed using ISO 527-2 5B specimens on a TestResources universal testing machine. The mass fraction of cross-linker **DA-PEG-1** in the resin has substantial effects on the viscoelastic properties of the ionogels. The data in Fig. 2a shows that with increasing mass fraction of **DA-PEG-1**, the Young's modulus decreases and the ionogels show lower nominal tensile strain prior to failure. The Young's moduli for 10-BVIM, 15-BVIM, and 20-BVIM were 739.3 ± 217.9 kPa, 119.1 ± 18.7 kPa, and 67.3 ± 16.2 kPa, respectively, and the corresponding strains at break were 1184.9 ± 121.5%, 860.6 ± 21.1%, and 693.5 ± 33.2% (Table S6†). The

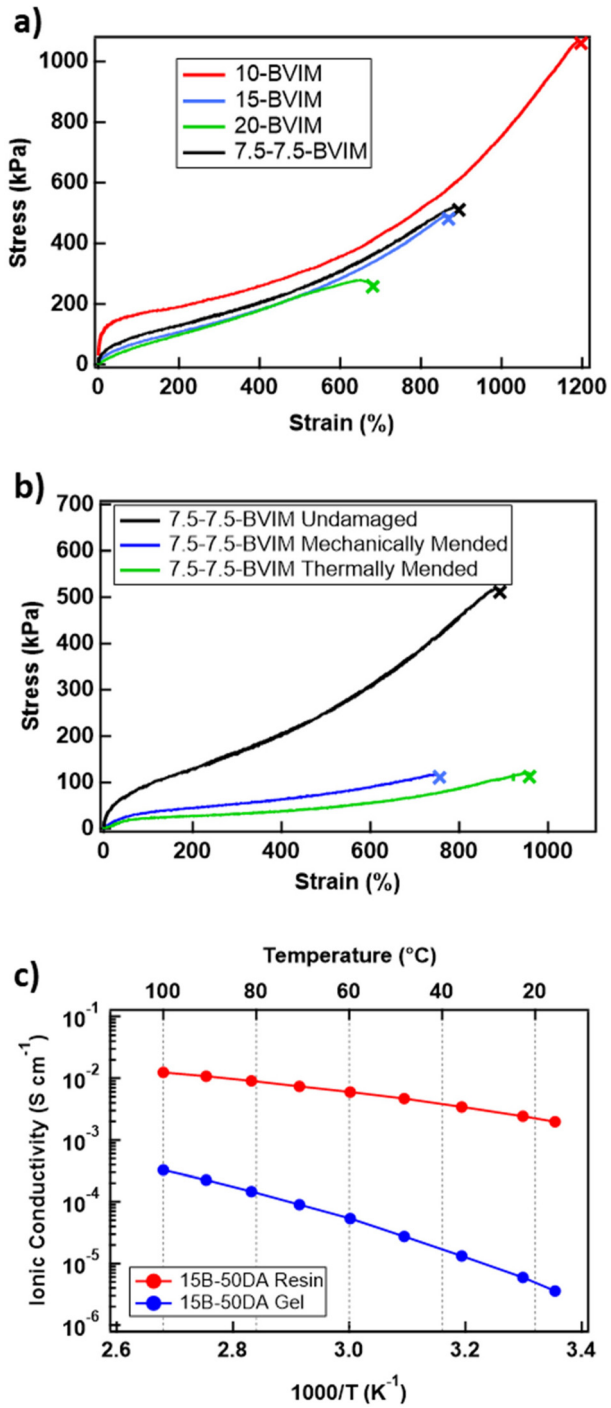

Fig. 2 Characterization of ionic liquid gels. (a) Tensile strength of gels with varying amounts of copolymer. (b) Tensile experiments of formulation 7.5–7.5-BVIM after printing, after being cut and mechanically mended (pushed together), and after being thermally mended at 85 °C. (c) Electrical Impedance Spectroscopy (EIS) data of formulation 7.5–7.5-BVIM as a resin (red) and after printing (blue) over a range of temperatures (20–100 °C).

decrease in elongation at break is consistent with a higher degree of chemical cross-linking in the polymer network. The decrease in Young's modulus is likely due to the plasticizing effect of PEG, which has been shown to improve the chain mobility of polymerized ionic liquid networks.[36,57,58] For 7.5–7.5-BVIM gels, the Young's modulus was 235.7 ± 25.3 kPa and the strain at break was 898.0 ± 30.2% (Fig. 2a). The increased Young's modulus relative to 15-BVIM is due to the presence of permanent crosslinks, while the similar strain at break is because both networks possess the same w/w% of crosslinker.

We next investigated the ability of these networks to remodel at the interface between two different substrates. Tensile specimens were printed, cut in half, and mended either mechanically (pushed together) or thermally. Interestingly, the Young's modulus is comparable between the mechanically reattached and thermally treated samples. As expected, both of these values are lower relative to the original sample before cutting due to the loss of the permanent cross-links within the network. Tensile specimens of 7.5–7.5-BVIM which had been cut and mended thermally exhibited a larger strain at break (1086.3 ± 180.7%) compared to samples which were cut and mechanically reattached (773.6 ± 34.4%) (Fig. 2b). This difference can be attributed to a greater number of Diels–Alder cross-links re-forming across the damaged interface. In comparison, we observed a similar trend for mechanically mended 15-BVIM samples, which exhibited a strain at break of 240.0 ± 27.7% *versus* the thermally mended 15-BVIM samples which improved to 654.9 ± 22.5%.

A crucial element of any material intended for sensing is its conductivity. Electrical impedance spectroscopy (EIS) measurements carried out on an Autolab 302N potentiostat galvanostat (Fig. 2c) demonstrated the material is conductive both as a resin and as a printed gel. Conductivity in the cured material is decreased due to immobilization of the IL.

Stress relaxation experiments were performed to determine the relaxation time across a range of temperatures from 75 °C to 105 °C (Fig. 3a). A 5% strain was applied to the network, and the relaxation times were determined by using the normalized modulus of the sample at $1/e$ of its initial value. This data was plotted *versus* $1000/T$ to determine an activation energy for the Diels–Alder adducts of 84 ± 5 kJ mol^{-1} (Fig. 3b). This value is similar to those reported in the literature that had a range of 98–115 kJ mol^{-1}.[59] The position of the functional groups on furan and maleimide derivatives, as well as the solvent, are known to strongly influence the activation energy of the reverse Diels–Alder reaction and can lead to the range of values observed.

To explore the suitability of the resin formulations for producing mechanically robust modular piezoionic sensors, blocks in the shape of a cube, bent arm, and cross, were printed and arranged into a linear, cyclic, or cubic configurations (Fig. 4). Blocks composed of 10-BVIM, 15-BVIM, or 20-BVIM were placed in contact with one another and heated at 60 °C overnight to initiate the reversible Diels–Alder reaction at the interface between the blocks. The modular pieces were successfully fused into one continuous structure, however, there was a significant loss in the resolution of the printed shape when PEG-BUM was not included in the resin formulation. Heating the dynamic networks above their T_g and

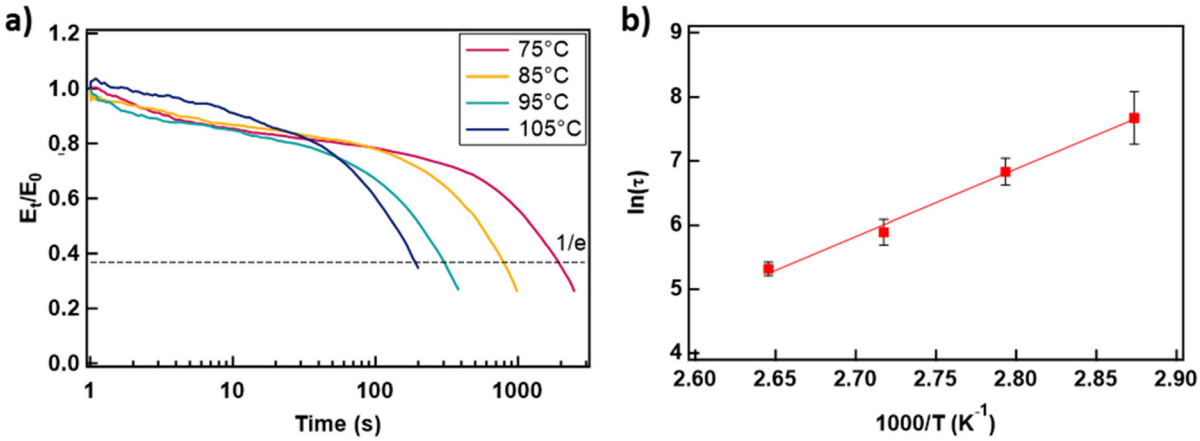

Fig. 3 (a) Stress relaxation of 7.5–7.5-BVIM gels at varying temperatures. Relaxation times (τ) are determined when the normalized modulus reaches 1/*e* of the initial value. (b) Activation energy (E_a) of Diels–Alder bonds in the network was determined from the slope of the natural logarithm of τ plotted against 1000/*T* (E_a = 84 ± 5 kJ mol^{-1}).

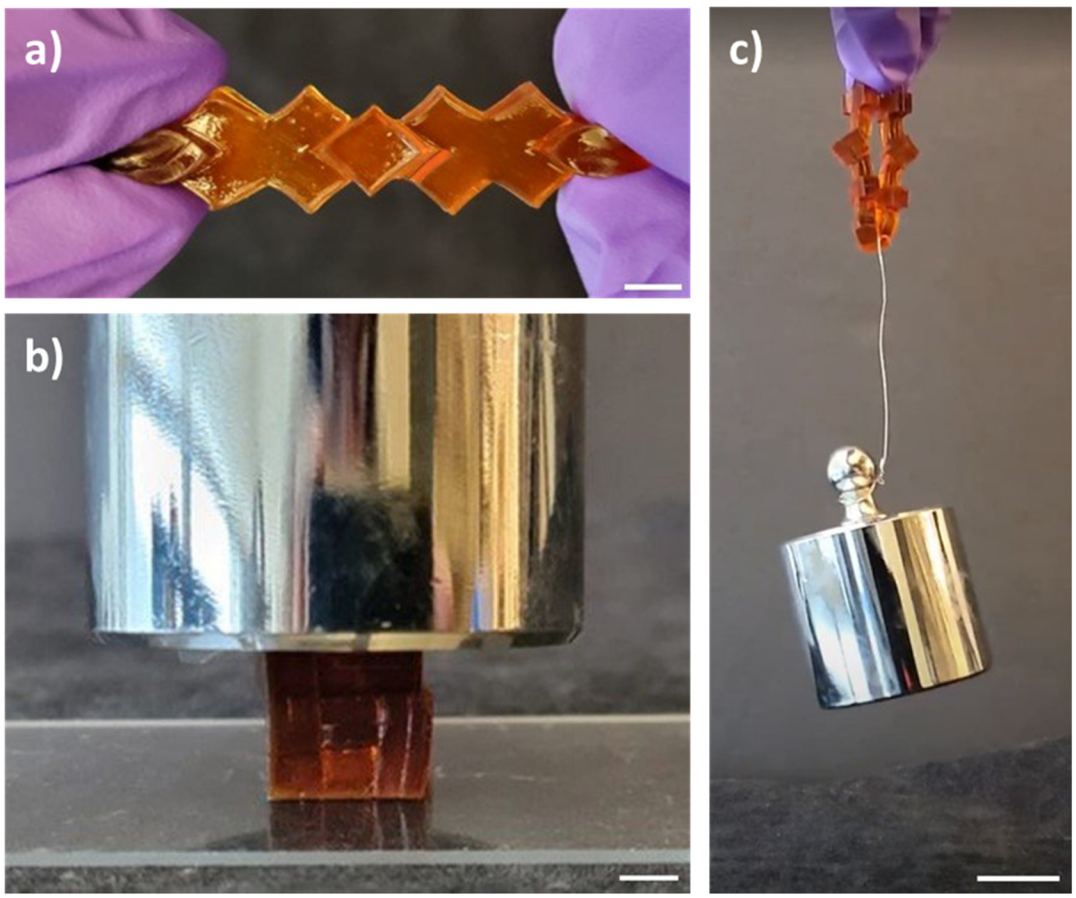

Fig. 4 Demonstration of the mechanical robustness of assembled and fused piezoionic sensors as a (a) linear, (b) box, and (c) loop. The weight shown is 500 g. The scale bar for linear and box structures represents 5 mm. Scale bar for loop represents 20 mm.

under fast Diels–Alder exchange caused the material to reflow under the forces of gravity (ESI†). In contrast, the 7.5–7.5-BVIM ionogels successfully maintained their shape fidelity as a consequence of the non-reversible cross-links present in the network. Heating these samples at 85 °C for 4.5 h was sufficient to fuse the polymer networks at the interface between two modular building blocks without diminishing the resolution of the printed features.

We investigated the hysteresis in these materials over multiple deformation cycles.[13–16] Cyclic uniaxial tensile experiments show the hysteresis of 7.5–7.5-BVIM gels under different strain rates ranging from 5 to 100 mm min^{-1} at 50% strain (Fig. 5a). The results showed that sensors stretched at slower strain rates experienced lower amounts of hysteresis and lower stress values because the network had more time to relax between cycles. When the material was stretched at higher strain rates, more force was required, and a larger hysteresis was observed. In all cases, the greatest amount of hysteresis was observed between the first and second cycles and decreased significantly after the second cycle. Similarly, when the sensors were stretched at a constant strain rate of 50 mm min^{-1} at strains ranging from 5–100%, lower amounts of strain resulted in smaller hysteresis and lower stress (Fig. 5b, Fig. S16†). As the % strain increased, the stress experienced by the network increased along with a slight increase in hysteresis.

In order to examine the performance of the modular sensors, conductivity measurements were performed with a Keithley 2400 source measure unit (SMU). Blocks of 7.5–7.5-BVIM were first fused into a loop-shaped structure. Electrodes

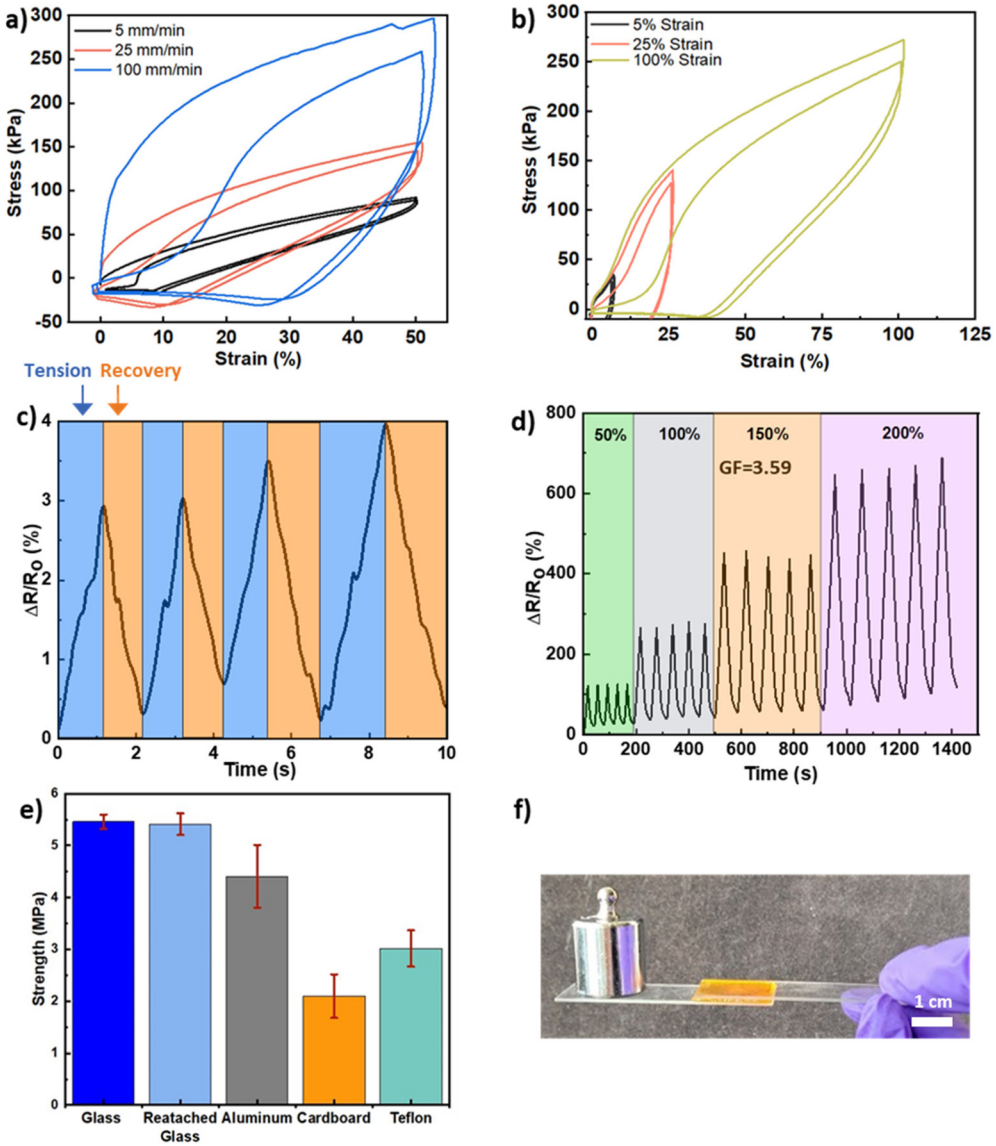

Fig. 5 Dynamic properties of modular sensors. (a) Cyclic uniaxial tensile experiments performed at strain rates of 5, 25, and 100 mm min^{-1} at 50% strain; two cycles for each strain rate are shown and additional cycles are included in the ESI.† (b) Cyclic uniaxial tensile experiments performed at 5%, 25%, and 100% strain at a strain rate of 50 mm min^{-1}; two cycles for each % strain are shown and additional cycles are included in the ESI.† (c) Electrical response of sensors attached to a source measuring unit, applying a 5% of strain. Current passing through the device decreases as the device is placed under tension, as predicted by modified Ohm's Law. (d) A plot showing the cyclic loading and unloading to different strains to determine the gauge factor for strains ranging from 50–200%. (e) Adhesive strength of 7.5–7.5-BVIM gels in contact with a variety of substrates. (f) Square adhesive ion gel patch supporting a 100 g weight on glass slides.

were attached to opposite ends of the loop and connected to the SMU (Fig. S15†). Stretching the loop provokes a decrease in the measured current. The decrease in current is a result of an increase in length and a decrease in the cross-sectional area of the structure as described by the equation:

$$\frac{V}{I} = \rho\frac{L}{A}$$

which relates resistance (R), resistivity (ρ), length (L) and cross-sectional area (A) of the sample. Since the applied voltage and resistivity are constant, the current drops in response to the deformation. Once the applied strain is removed, the current increases (Fig. 5c). To evaluate the performance of a piezoionic device under compression, printed blocks were arranged into a box configuration and thermally cured into a continuous network structure. The box was connected to the SMU using electrodes and copper plates (Fig. S15†). As expected, compression led to an increase in current due to the decrease in the shortest path between the electrodes. The strain-dependent sensitivity of the sensors is evaluated as the gauge factor (GF), which is the ratio of change in electrical resistance to applied mechanical strain The GF was 2.08 under 5–50% strain (Fig. S27†), which increased to 3.59 under 50–200% strain (Fig. 5d). Larger strains cause a larger deformation to the network, which interrupts conductive pathways by increasing the separation between anions and cations, leading to higher resistance.[34] The GF for our system was comparable or higher than those reported in the literature for other ionogels.[60–65]

All of the ionogels also exhibited an adhesive character, which was characterized using lap-shear adhesion tests. The adhesive strength of the ionogels were evaluated for glass, aluminum, cardboard, and Teflon substrates (Fig. 5e). The gels adhered best to glass (5.45 MPa) and maintained their adhesive strength after being detached and reapplied (5.37 MPa). The strong adhesive properties of these materials are attributed to the broad range of noncovalent interactions (hydrogen bonding, electrostatic, ion-dipole, and van der Waals interactions) between the ion gels and the substrate.[9,18,66,67] The adhesion to different substrate types could be advantageous for these sensors to remain in place once they are installed.

Conclusion

A photopolymerizable ionic liquid resin was developed for 3D printing ionogel CANs that can be fused together to create piezoionic sensors. During the 3D printing process, the resin was transformed into dynamic ionogel networks, wherein Diels–Alder adducts were utilized to create reversible crosslinks. The printed structures demonstrate high print quality, as well as desirable mechanical properties such as good elasticity (1184% strain at break) and strength (739 kPa), which can be tuned by altering the number of dynamic crosslinks in the material. These dynamic covalent bonds imbued a mechanism for self-repair in the material and were also active at the substrate surface, such that two different 3D printed networks could be fused into a single continuous network. Within these ionogels, the unpolymerized ionic liquid is mobile within the network. Thus, the printed and fused ionogels were conductive and performed as piezoionic sensors. As a representative demonstration, three different modular building blocks were 3D printed. Using these building blocks, an end-user can assemble a piezoionic sensor with any arbitrary design, as necessary. This strategy, wherein 3D printed parts can be assembled into a larger functional system, showcases a decentralized manufacturing approach for future on-demand production of active devices.

Conflicts of interest

The authors declare no competing financial interest.

Acknowledgements

This research is financially supported by the Center for the Chemistry of Molecularly Optimized Networks (MONET), a National Science Foundation (NSF) Center for Chemical Innovation (CHE-2116298). We gratefully acknowledge support from the U.S. Army Research Office (W911NF-17-1-0595) for N. B. on this project.

References

1 C. Zhang, B. He, Z. Wang, Y. Zhou, A. Ming and N. Thanh Dinh, Application and Analysis of an Ionic Liquid Gel in a Soft Robot, *Adv. Mater. Sci. Eng.*, 2019, 2857282.
2 C. Zhang, B. He, A. Ding, S. Xu, Z. Wang and Y. Zhou, Motion Simulation of Ionic Liquid Gel Soft Actuators Based on CPG Control, *Comput. Intell. Neurosci.*, 2019, 8256723.
3 A. Ankit, N. Tiwari, F. Ho, F. Krisnadi, M. R. Kulkarni, L. L. Nguyen, S. J. A. Koh and N. Mathews, High-k, Ultrastretchable Self-Enclosed Ionic Liquid-Elastomer Composites for Soft Robotics and Flexible Electronics, *ACS Appl. Mater. Interfaces*, 2020, **12**(33), 37561–37570.
4 R. L. Truby, M. Wehner, A. K. Grosskopf, D. M. Vogt, S. G. M. Uzel, R. J. Wood and J. A. Lewis, Soft Somatosensitive Actuators via Embedded 3D Printing, *Adv. Mater.*, 2018, **30**(15), 1706383.
5 B. He, Y. Zhou, Z. Wang, Q. Wang, R. Shen and S. Wu, A Multi-Layered Touch-Pressure Sensing Ionogel Material Suitable for Sensing Integrated Actuations of Soft Robots, *Sens. Actuators, A*, 2018, **272**, 341–348.
6 C. Feng, C. P. Hemantha Rajapaksha and A. Jákli, Ionic Elastomers for Electric Actuators and Sensors, *Engineering*, 2021, **7**(5), 581–602.
7 Z. Liu, Y. Wang, Y. Ren, G. Jin, C. Zhang, W. Chen and F. Yan, Poly(Ionic Liquid) Hydrogel-Based Anti-Freezing Ionic Skin for a Soft Robotic Gripper, *Mater. Horiz.*, 2020, **7**(3), 919–927.

8 W. Gao, H. Ota, D. Kiriya, K. Takei and A. Javey, Flexible Electronics toward Wearable Sensing, *Acc. Chem. Res.*, 2019, **52**(3), 523–533.
9 S. Hao, T. Li, X. Yang and H. Song, Ultrastretchable, Adhesive, Fast Self-Healable, and Three-Dimensional Printable Photoluminescent Ionic Skin Based on Hybrid Network Ionogels, *ACS Appl. Mater. Interfaces*, 2022, **14**(1), 2029–2037.
10 N. Gao, Y. He, X. Tao, X. Q. Xu, X. Wu and Y. Wang, Crystal-Confined Freestanding Ionic Liquids for Reconfigurable and Repairable Electronics, *Nat. Commun.*, 2019, **10**(1), 547.
11 J. Tie, Z. Mao, L. Zhang, Y. Zhong, X. Sui and H. Xu, Highly Transparent, Self-Healing and Adhesive Wearable Ionogel as Strain and Temperature Sensor, *Polym. Chem.*, 2022, **13**, 4064–4075.
12 A. Basu, J. Wong, B. Cao, N. Boechler, A. J. Boydston and A. Nelson, Mechanoactivation of Color and Autonomous Shape Change in 3D-Printed Ionic Polymer Networks, *ACS Appl. Mater. Interfaces*, 2021, **13**, 19263–19270.
13 R. Borayek, F. Foroughi, X. Xin, A. M. Mohamed, M. M. Abdelrahman, M. Zedan, D. Zhang and J. Ding, Near-Zero Hysteresis Ionic Conductive Elastomers with Long-Term Stability for Sensing Applications, *ACS Appl. Mater. Interfaces*, 2022, **14**(9), 11727–11738.
14 D. Y. Choi, M. H. Kim, Y. S. Oh, S. H. Jung, J. H. Jung, H. J. Sung, H. W. Lee and H. M. Lee, Highly Stretchable, Hysteresis-Free Ionic Liquid-Based Strain Sensor for Precise Human Motion Monitoring, *ACS Appl. Mater. Interfaces*, 2017, **9**(2), 1770–1780.
15 J. Wong, A. T. Gong, P. A. Defnet, L. Meabe, B. Beauchamp, R. M. Sweet, H. Sardon, C. L. Cobb and A. Nelson, 3D Printing Ionogel Auxetic Frameworks for Stretchable Sensors, *Adv. Mater. Technol.*, 2019, **4**(9), 1–6.
16 K. Tian, J. Bae, S. E. Bakarich, C. Yang, R. D. Gately, G. M. Spinks, M. in het Panhuis, Z. Suo and J. J. Vlassak, 3D Printing of Transparent and Conductive Heterogeneous Hydrogel–Elastomer Systems, *Adv. Mater.*, 2017, **29**(10), 28075033.
17 M. Jurinovs, A. Barkane, O. Platnieks, L. Grase and S. Gaidukovs, Three Dimensionally Printed Biobased Electrodes: Ionic Liquid and Single-Walled Carbon Nanotube Hybrids in a Vegetable Oil Matrix for Soft Robotics, *ACS Appl. Polym. Mater.*, 2023, **5**(9), 7120–7131.
18 J. Zhang, Z. Chen, Y. Zhang, S. Dong, Y. Chen and S. Zhang, Poly(Ionic Liquid)s Containing Alkoxy Chains and Bis(Trifluoromethanesulfonyl)Imide Anions as Highly Adhesive Materials, *Adv. Mater.*, 2021, **33**(30), 1–10.
19 X. Fan, S. Liu, Z. Jia, J. J. Koh, J. C. C. Yeo, C. G. Wang, N. E. Surat'man, X. J. Loh, J. Le Bideau, C. He, *et al.*, Ionogels: Recent Advances in Design, Material Properties and Emerging Biomedical Applications, *Chem. Soc. Rev.*, 2023, **52**(7), 2497–2527.
20 Q. Shen, M. Jiang, R. Wang, K. Song, M. Hou Vong, W. Jung, F. Krisnadi, R. Kan, F. Zheng, B. Fu, *et al.*, Liquid Metal-Based Soft, Hermetic, and Wireless-Communicable Seals for Stretchable Systems, *Science*, 2023, **379**(6631), 488–493.
21 J. Xu, Z. Wang, X. Wang, Y. Wu, R. Xing, T. Yu, Y. Li, J. Ao, Y. Tao, B. Bai, *et al.*, Breathable Encapsulated Liquid Metal Foam-Based Soft Stress Sensor, *Adv. Mater. Technol.*, 2023, **8**(6), 2201193.
22 S. C. B. Mannsfeld, B. C. K. Tee, R. M. Stoltenberg, C. V. H. H. Chen, S. Barman, B. V. O. Muir, A. N. Sokolov, C. Reese and Z. Bao, Highly Sensitive Flexible Pressure Sensors with Microstructured Rubber Dielectric Layers, *Nat. Mater.*, 2010, **9**(10), 859–864.
23 M. Yeol Lee, H. Rang Lee, C. Hee Park, S. Gi Han and J. Hak Oh, Organic Transistor-Based Chemical Sensors for Wearable Bioelectronics, *Acc. Chem. Res.*, 2018, **51**(11), 2829–2838.
24 Z. Shen, W. Huang, L. Li, H. Li, J. Huang, J. Cheng and Y. Fu, Research Progress of Organic Field-Effect Transistor Based Chemical Sensors, *Small*, 2023, 2302406.
25 K. Liu, B. Ouyang, X. Guo, Y. Guo and Y. Liu, Advances in Flexible Organic Field-Effect Transistors and Their Applications for Flexible Electronics, *npj Flexible Electron.*, 2022, **6**(1), 1.
26 J. B. Chossat, H. S. Shin, Y. L. Park and V. Duchaine, Soft Tactile Skin Using an Embedded Ionic Liquid and Tomographic Imaging, *J. Mech. Rob.*, 2015, **7**(2), 021008.
27 J. Wong, A. Basu, M. Wende, N. Boechler and A. Nelson, Mechano-Activated Objects with Multidirectional Shape Morphing Programmed via 3D Printing, *ACS Appl. Polym. Mater.*, 2020, **2**(7), 2504–2508.
28 W. Kunz and K. Häckl, The Hype with Ionic Liquids as Solvents, *Chem. Phys. Lett.*, 2016, **661**, 6–12.
29 Y. M. Kim, J. H. Kwon, S. Kim, U. H. Choi and H. C. Moon, Ion-Cluster-Mediated Ultrafast Self-Healable Ionoconductors for Reconfigurable Electronics, *Nat. Commun.*, 2022, **13**(1), 3769.
30 M. Rebei, A. Mahun, Z. Walterova, O. Trhlikova, R. K. Donato and H. Beneš, VOC-Free Tricomponent Reaction Platform for Epoxy Network Formation Mediated by a Recyclable Ionic Liquid, *Polym. Chem.*, 2022, **13**, 5380–5388.
31 S. Livi, J. Baudoux, J. F. Gérard and J. Duchet-Rumeau, Ionic Liquids: A Versatile Platform for the Design of a Multifunctional Epoxy Networks 2.0 Generation, *Prog. Polym. Sci.*, 2022, **132**, 101581.
32 C. G. Cassity, A. Mirjafari, N. Mobarrez, K. J. Strickland, R. A. O'brien and J. H. Davis, Ionic Liquids of Superior Thermal Stability, *Chem. Commun.*, 2013, **49**(69), 7590–7592.
33 M. Wang, P. Zhang, M. Shamsi, J. L. Thelen, W. Qian, V. K. Truong, J. Ma, J. Hu and M. D. Dickey, Tough and Stretchable Ionogels by in Situ Phase Separation, *Nat. Mater.*, 2022, **21**(3), 359–365.
34 X. Zhao, J. Xu, J. Zhang, M. Guo, Z. Wu, Y. Li, C. Xu, H. Yin and X. Wang, Fluorescent Double Network Ionogels with Fast Self-Healability and High Resilience for Reliable Human Motion Detection, *Mater. Horiz.*, 2022, **10**, 646–656.

35 Z. J. Chen, Y. Q. Sun, X. Xiao, H. Q. Wang, M. H. Zhang, F. Z. Wang, J. C. Lai, D. S. Zhang, L. J. Pan and C. H. Li, An Ultra-Tough and Ultra-Sensitive Ionogel Pressure/Temperature Sensor Enabled by Hierarchical Design of Both Materials and Devices, *J. Mater. Chem. A*, 2023, **11**(15), 8359–8367.

36 B. Narupai, J. Wong, E. Sanchez-Rexach, J. Smith-Jones, V. C. T. Le, N. Sadaba, H. Sardon and A. Nelson, 3D Printing of Ionic Liquid Polymer Networks for Stretchable Conductive Sensors, *Adv. Mater. Technol.*, 2023, **2300226**, 1–9.

37 S. Amziane, A. Pierre, D. Rangeard, M. Sonebi and A. Perrot, *3D Printing of Concrete: State of the Art and Challenges of the Digital Construction Revolution*, 2019.

38 R. L. Truby and J. A. Lewis, Printing Soft Matter in Three Dimensions, *Nature*, 2016, **540**(7633), 371–378.

39 M. R. Hartings and Z. Ahmed, Chemistry from 3D Printed Objects, *Nat. Rev. Chem.*, 2019, **3**, 305–314.

40 T. J. Wallin, J. Pikul and R. F. Shepherd, 3D Printing of Soft Robotic Systems, *Nat. Rev. Mater.*, 2018, **3**(6), 84–100.

41 A. J. Capel, R. P. Rimington, M. P. Lewis and S. D. R. Christie, 3D Printing for Chemical, Pharmaceutical and Biological Applications, *Nat. Rev. Chem.*, 2018, **2**(12), 422–436.

42 A. H. Espera, J. R. C. Dizon, Q. Chen and R. C. Advincula, 3D-Printing and Advanced Manufacturing for Electronics, *Prog. Addit. Manuf.*, 2019, **4**, 245–267.

43 H. W. Tan, Y. Y. C. Choong, C. N. Kuo, H. Y. Low and C. K. Chua, 3D Printed Electronics: Processes, Materials and Future Trends, *Prog. Mater. Sci.*, 2022, 100945.

44 G. L. Goh, H. Zhang, T. H. Chong and W. Y. Yeong, 3D Printing of Multilayered and Multimaterial Electronics: A Review, *Adv. Electron. Mater.*, 2021, 2100445.

45 Z. Wang, J. Zhang, J. Liu, S. Hao, H. Song and J. Zhang, 3D Printable, Highly Stretchable, Superior Stable Ionogels Based on Poly(Ionic Liquid) with Hyperbranched Polymers as Macro-Cross-Linkers for High-Performance Strain Sensors, *ACS Appl. Mater. Interfaces*, 2021, **13**(4), 5614–5624.

46 C. D. Onal and D. Rus, A Modular Approach to Soft Robots, in *Proceedings of the IEEE RAS and EMBS International Conference on Biomedical Robotics and Biomechatronics*, 2012, 1038–1045.

47 C. Zhang, P. Zhu, Y. Lin, Z. Jiao and J. Zou, Modular Soft Robotics: Modular Units, Connection Mechanisms, and Applications, *Adv. Intell. Syst.*, 2020, **2**(6), 1900166.

48 S. A. Morin, Y. Shevchenko, J. Lessing, S. W. Kwok, R. F. Shepherd, A. A. Stokes and G. M. Whitesides, Using "Click-e-Bricks" to Make 3D Elastomeric Structures, *Adv. Mater.*, 2014, **26**(34), 5991–5999.

49 E. F. Gomez, S. V. Wanasinghe, A. E. Flynn, O. J. Dodo, J. L. Sparks, L. A. Baldwin, C. E. Tabor, M. F. Durstock, D. Konkolewicz and C. J. Thrasher, 3D-Printed Self-Healing Elastomers for Modular Soft Robotics, *ACS Appl. Mater. Interfaces*, 2021, **13**, 28870–28877.

50 C. Bowman, F. Du Prez and J. Kalow, Introduction to Chemistry for Covalent Adaptable Networks, *Polym. Chem.*, 2020, **11**(33), 5295–5296.

51 C. J. Kloxin, T. F. Scott, B. J. Adzima and C. N. Bowman, Covalent Adaptable Networks (CANs): A Unique Paradigm in Cross-Linked Polymers, *Macromolecules*, 2010, **43**, 2643.

52 J. V. Accardo and J. A. Kalow, Reversibly Tuning Hydrogel Stiffness through Photocontrolled Dynamic Covalent Crosslinks, *Chem. Sci.*, 2018, **9**(27), 5987–5993.

53 S. Gulyuz, Y. Yagci and B. Kiskan, Exploiting the Reversible Covalent Bonding of Boronic Acids for Self-Healing/Recycling of Main-Chain Polybenzoxazines, *Polym. Chem.*, 2022, **13**(24), 3631–3638.

54 W. Thongsomboon, M. Sherwood, N. Arellano and A. Nelson, Thermally Induced Nanoimprinting of Biodegradable Polycarbonates Using Dynamic Covalent Cross-Links, *ACS Macro Lett.*, 2013, **2**(1), 19–22.

55 S. Jung, S. Y. Kim, J. C. Kim, S. M. Noh and J. K. Oh, Ambient Temperature Induced Diels-Alder Crosslinked Networks Based on Controlled Methacrylate Copolymers for Enhanced Thermoreversibility and Self-Healability, *RSC Adv.*, 2017, **7**(42), 26496–26506.

56 S. C. Millik, A. M. Dostie, D. G. Karis, P. T. Smith, M. McKenna, N. Chan, C. D. Curtis, E. Nance, A. B. Theberge and A. Nelson, 3D Printed Coaxial Nozzles for the Extrusion of Hydrogel Tubes toward Modeling Vascular Endothelium, *Biofabrication*, 2019, **11**(4), 045009.

57 H. Kokubo, R. Sano, K. Murai, S. Ishii and M. Watanabe, Ionic Polymer Actuators Using Poly(Ionic Liquid) Electrolytes, *Eur. Polym. J.*, 2018, **106**, 266–272.

58 R. Zhao, J. Yang, B. Wang, Z. Ma, L. Pan and Y. Li, Block Copolymer Solid Electrolytes Based on Comb-Like Poly(Ethylene Glycol) Plasticized Poly(Ionic Liquid)s for Lithium-Ion Batteries, *Chin. J. Chem.*, 2023, **41**(19), 2493–2501.

59 K. C. Koehler, A. Durackova, C. J. Kloxin and C. N. Bowman, Kinetic and Thermodynamic Measurements for the Facile Property Prediction of Diels-Alder-Conjugated Material Behavior, *AIChE J.*, 2012, **58**(11), 3545–3552.

60 M. Zhang, R. Yu, X. Tao, Y. He, X. Li, F. Tian, X. Chen and W. Huang, Mechanically Robust and Highly Conductive Ionogels for Soft Ionotronics, *Adv. Funct. Mater.*, 2023, 2208083.

61 Q. Wu, Y. Xu, S. Han, J. Zhu, A. Chen, J. Zhang, Y. Chen, X. Yang, J. Huang and L. Guan, A Liquid-Free Conducting Ionoelastomer for 3D Printable Multifunctional Self-Healing Electronic Skin with Tactile Sensing Capabilities, *Mater. Horiz.*, 2023, **5**(10), 3610–3621.

62 C. Wang, J. Zhang, C. Niu, Q. Fu and L. Lu, Dual-Mechanism-Driven Environmental-Friendly Fast Self-Healing Ionic Hydrogels with Excellent Sensitivity to Strain Responsiveness, *Chem. Mater.*, 2023, **35**(5), 1991–2005.

63 S. Wu, J. Huang, S. Jing, H. Xie and S. Zhou, Biodegradable Shape-Memory Ionogels as Green and Adaptive Wearable Electronics Toward Physical Rehabilitation, *Adv. Funct. Mater.*, 2023, 2303292.

64 X. Zhao, J. Xu, J. Zhang, M. Guo, Z. Wu, Y. Li, C. Xu, H. Yin and X. Wang, Fluorescent Double Network Ionogels with Fast Self-Healability and High Resilience for Reliable Human Motion Detection, *Mater. Horiz.*, 2022, **10**, 646–656.

65 C. Choi, Y. Lee, K. W. Cho, J. H. Koo and D. H. Kim, Wearable and Implantable Soft Bioelectronics Using Two-Dimensional Materials, *Acc. Chem. Res.*, 2019, **52**(1), 73–81.
66 Q. Xia, W. Li, X. Zou, S. Zheng, Z. Liu, L. Li and F. Yan, Metal-Organic Frameworks (MOFs) Facilitated Highly Stretchable, and Fatigue-Resistant Ionogels for Recyclable Sensors, *Mater. Horiz.*, 2022, **9**, 2881–2892.
67 J. Zhu, X. Lu, W. Zhang and X. Liu, Substrate-Independent, Reversible, and Easy-Release Ionogel Adhesives with High Bonding Strength, *Macromol. Rapid Commun.*, 2020, **41**(24), 2000098.